Thermal Embrittlement of Simulated Heat-Affected Zone in Cast Austenitic Stainless Steels

The heat-affected zone is more susceptible intrinsically to thermal embrittlement than the parent casting

BY H. MIMURA, T. TANIGUCHI, Y. HORII, R. KUME AND N. UESUGI

ABSTRACT. Metallurgical factors controlling thermal embrittlement in the heat-affected zone (HAZ) of cast austenitic stainless steels were investigated by using the simulated HAZ. It was shown that the simulated HAZ was more susceptible to the thermal embrittlement by aging at 673 K in correspondence with its higher tendency to age hardening and a higher content of ferrite than the parent casting. Electron microprobe analyzer (EPMA) measurement showed that application of the simulated thermal cycle gave a change in the chemical composition of the ferrite, which might be a cause of the higher age hardening of the ferrite in the simulated HAZ. This higher ferrite hardness had a good correlation with fine precipitates of presumably G-phase in the ferrite grain, which existed more in the simulated HAZ than in the parent casting, though it is not clear whether this correlation was only apparent. Ductility of the austenite portion was found to reduce remarkably when surrounded by the hard ferrite of a high fraction. Annealing after aging restored CTOD to some degree. Aging after fatigue cracking gave more embrittlement than a usual procedure for preparation of test specimens, *i.e.*, fatigue cracking after aging.

Introduction

Cast austenitic stainless steels with weld joints are used for primary coolant circuits in pressurized water reactors. Under operating conditions, the austenitic stainless steels suffer embrittlement due to aging at temperatures in the range of 563–598 K. By using Charpy tests on parent castings and weld joints, Strangwood and Druce showed that the heat-affected zone (HAZ) in full aging condition has the highest transition temperature among the parent castings, HAZ and the weld metal (Ref. 1). Therefore, an assessment of the structural integrity should be made based on HAZ toughness, and clarification of metallurgical factors making HAZ brittle is essential. The latter is the purpose of the present work.

Measurement of HAZ toughness using weld joints is suitable for the former, but not appropriate for the latter for the following reason: The measured HAZ toughness value of the weld joint is affected not only by metallurgical factors but also by mechanical ones, such as plastic constraint by weld metals of overmatching, variety of toughness and strength in HAZ, and crack path deviation from HAZ to weld metal. These mechanical effects on toughness are too complex to be evaluated quantitatively. In addition, it is not always easy to position the crack tip at the most embrittled portion of HAZ in weld joints. To avoid such ambiguity, the present work employed the simulated HAZ toughness that is controlled by metallurgical factors alone. The effect of aging was studied for materials aged at 673 K for periods up to 28.8 Ms, using transmission electron microscopy (TEM), energy dispersive spectrometry (EDS), X-ray pole figure, electron microprobe analyzer (EPMA), microhardness, crack tip opening displacement (CTOD) testing and microfractography.

KEY WORDS

Age Hardening
Austenitic Stainless Steel
Charpy Test
CTOD Test
Ferrite
G Phase
Heat-Affected Zone

Test Methods

Two austenitic stainless steels conforming to the composition of CF8M in ACI code, #CF and #SC, were centrifugally cast into pipes and heated at 1363 K or 1353 K followed by water cooling. Ferrite content of the castings was about 15% for #CF, a typical fraction in CF8M, and about 25% for #SC, a somewhat high fraction in CF8M. Chemical compositions and mechanical properties of the castings are shown in Table 1.

The simulated HAZ specimens were prepared by the following procedure for heat treatment. The castings were machined into 11 × 11 × 55 mm blanks and subjected to HAZ thermal cycles composed of a single cycle or a double cycle by means of a Gleeble 1500 system. The maximum temperature of the single cycle, as well as the first cycle of the double cycle, was 1573 K, and those of the second cycle in the double cycles were 973 K, 1173 K and 1373 K. Constant cooling rates of 10 K/s, 20 K/s and 30 K/s were used for the single cycle and a rate of 30 K/s for the double cycle, effectively corresponding to those of fairly large heat input weldings.

Following the thermal cycling, half of the simulated HAZ specimens were machined to the final dimension for CTOD test specimens with the Charpy size with a 3-mm-length notch. Such small size specimens were suitable for thermal treatment and still useful enough for study on toughness, but insufficient for

H. MIMURA and T. TANIGUCHI are with the Yokohama National University, Japan; Y. HORII, R. KUME and N. UESUGI are with the Japan Power Engineering & Inspection Corporation, Japan.

Table 1 — Chemical Compositions and Mechanical Properties

Material	C	Si	Mn	P	S	Cr	Ni	Mo	N
#CF	0.06	0.74	0.75	0.027	0.008	20.0	10.7	2.12	0.038
#SC	0.05	1.26	0.69	0.016	0.008	20.3	9.10	2.24	0.034

Material	0.2% P.S. (MPa)	T.S. (MPa)	Elong. (%)	R.A.(%)	Heat Treatment
#CF	271	522	46	67	1363 K × 19.8 ks Water Cool
#SC	322	613	46	68	1353 K × 10.8 ks Water Cool

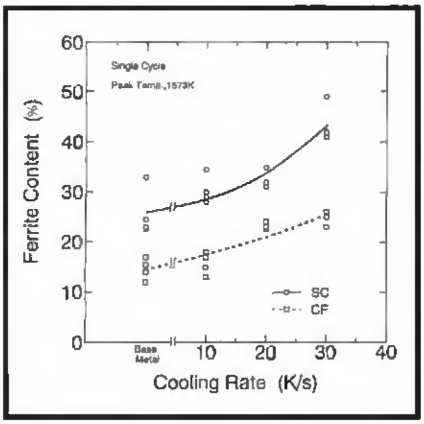

Fig. 1 — Effect of cooling rate on ferrite content in a single thermal cycle.

measurement of the plane strain fracture toughness. The remaining half of the simulated HAZ specimens were put in an electric furnace, aged at 673 K up to 28.8 Ms and machined as same. Although higher than the service temperature of 563–598 K, the present aging temperature of 673 K makes it possible to realize the thermal embrittlement in a relatively short aging period, keeping the same relationship between strength and toughness, which was shown to be valid for all specimens aged in a temperature range from 573–673 K (Ref. 2). However, the activation energy of the embrittlement process changes with temperature according to variation of contributions from metallurgical factors (Ref. 3).

Metallographical examination was made with an optical microscope to measure the ferrite/austenite balance by electrolytically etching the specimens in a 10% oxalic acid solution, using TEM to observe precipitates and lattice defects.

Micro-Vickers hardness with load of 25 gf was measured for both of the ferrite and austenite portions on the various stages of aging.

X-ray pole figure was studied using back reflection from the specimen of the size of the present CTOD specimen cross section.

The CTOD test was carried out with a three-point bending method in a gas-cooled or heated chamber in a temperature range from 103–323 K. The critical CTOD of three specimens expressed by δc, δu or δm was used as a measure of fracture toughness in the relevant temperature regions. Among them, δc or δu corresponds to the CTOD at the onset of unstable fracture (or pop-in) prior to or preceded by stable crack growth, respectively. The CTOD R-curve was obtained by means of the compliance method, by which the crack opening angle (COA) was evaluated. By the R curves, δc was discriminated from δu. The present steels showed successive minute load drops on a load vs. crack-mouth opening displacement curve in the transition temperature region. Distinction between the successive minute drops and the pop-in was not essential, but only conventional. When the unstable fracture or the pop-in was not observed, the CTOD corresponding to the maximum load was defined to be fracture toughness, expressed as δm.

A simple explanation of CTOD is given in the Appendix.

The fracture surface was observed with a scanning electron microscope (SEM). A cross section perpendicular to the fracture surface was examined with an optical microscope, SEM and TEM, for which a thin foil was prepared by thinning a Ni-plated fractured specimen with a focused ion beam (FIB).

Two additional studies on the effect of thermal history on toughness were done using the parent castings. The first was post annealing after aging to restore the thermal embrittlement. The second was exchange of the order of aging and fatigue notching. Both of the notching orders simulate the extreme cases of the actual situation in which fatigue crack may extend with progress of aging.

Test Results

The ratio of ferrite to austenite was clearly increased by application of the thermal cycle of the maximum temperature of 1573 K. When the higher cooling rate was employed, a higher ratio was obtained, as shown in Fig. 1. The morphology of ferrite was changed by the thermal cycle. More directional and angular ferrite structures, in part, were observed in the simulated HAZ of #SC, instead of vermicular ferrite in the parent castings, as shown in Fig. 2. Microstructure after aging at 673 K is shown in Fig. 3. Recognizable change in the ferrite content by aging was not found.

EPMA analysis showed that concentration of the ferrite-forming elements, such as Cr, Mo and Si, in the ferrite portion was elevated above the average value, as usual. Less elevation in the concentration of the elements was observed in the simulated HAZ than in the parent castings. The situation was reversed for the concentration of the austenite-forming element, Ni, in the ferrite portion. Examples of the concentration change are shown for Cr and Ni in Fig. 4. The change of the concentration in the ferrite by application of the thermal cycle was evaluated to be about, on an average, 30%, –10%, –10% and 0% of the concentration of the parent casting ferrite for Ni, Cr, Mo and Si, respectively.

Microhardness of ferrite did not show a definite change by application of the thermal cycle but increased drastically by aging in contrast to little change of microhardness of austenite, as shown in Fig. 5. In the figure, only the fair curves of the measured hardness are shown, except for the aged ferrite of #SC, for which all measured values of the microhardness are given as an example to indicate a degree of scatter. The increase in microhardness by aging was more remarkable in the simulated HAZ. Microhardness of ferrite increased with aging time in the early stage of the aging process, up to 3.6 Mc, in both of the parent casting and the simulated HAZ; microhardness continued to increase considerably in the simulated HAZ in the later stage, up to 28.8 Ms, as shown in Fig. 6.

It was shown with TEM that a few of

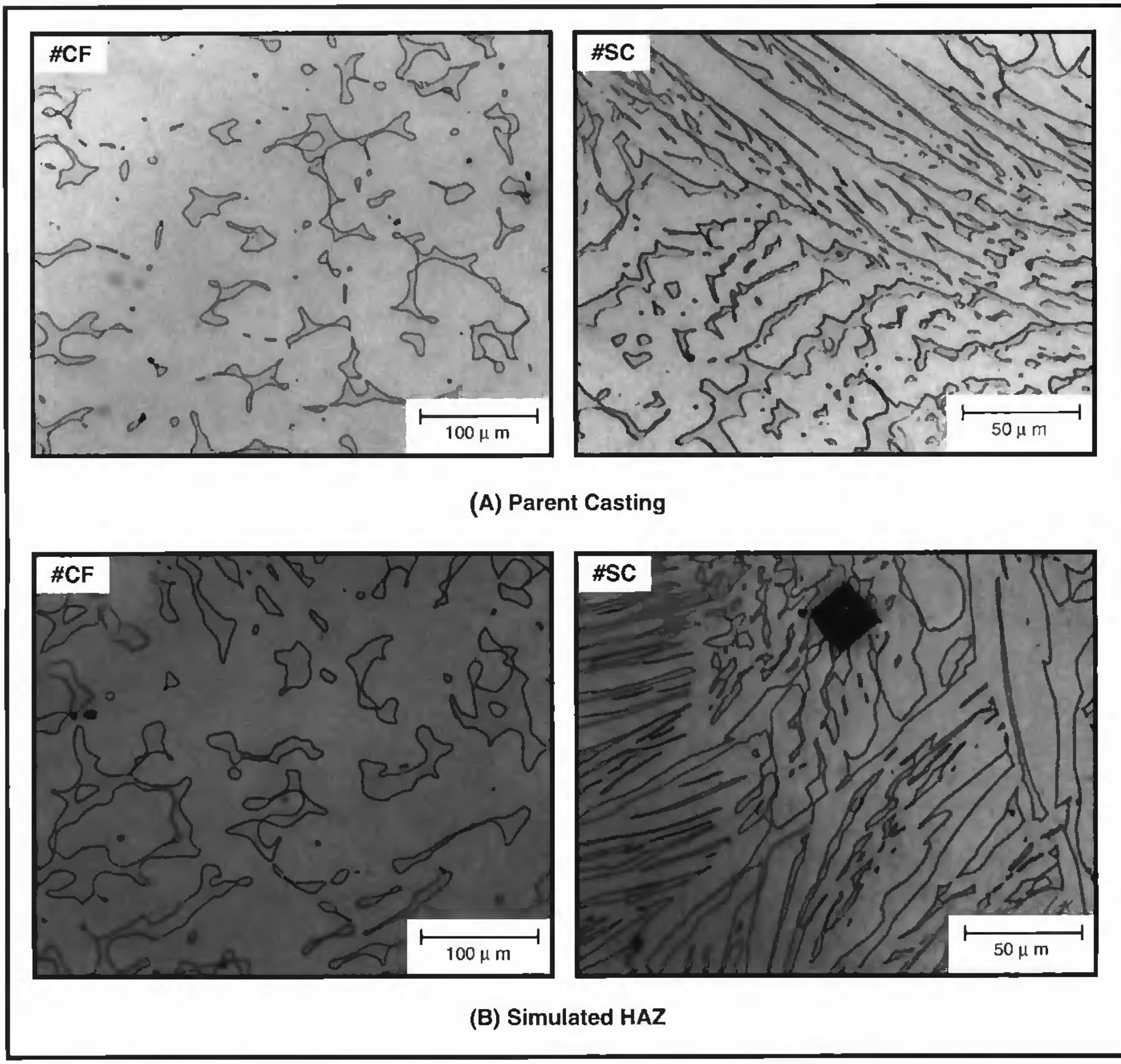

Fig. 2 — Microstructure of: A — Parent casting; and B — simulated HAZ subjected to a single cycle of cooling rate of 30 K/s.

$M_{23}C_6$-type carbides and Laves-like phase precipitates were observed along ferrite/austenite boundaries for the aged specimens. A few dislocation contrasts were detected for all specimens.

Note that fine precipitates were observed in the ferrite grain for the parent casting aged for 28.8 Ms, and for the simulated HAZ aged for 10.8 Ms and 28.8 Ms in #SC. Examples of dense precipitates observed with TEM of low and high magnification are shown in Fig. 7. They show the electron diffraction pattern of FCC structure, cube-on-cube orientation to delta ferrite with a lattice spacing of 1.12–1.14 nm, consistent with that of G phase, which varies with chemical composition (Ref. 4). Fine precipitates in the ferrite grain other than that of G phase are not known in CF8M aged at 673 K. Therefore, the fine precipitates were presumably of the G phase. When density of the precipitates was thin, sufficient numbers of the electron diffraction spots for judgment of a reciprocal lattice structure were not always observed. The morphology of the fine precipitates for various aging conditions were similar to each other. Therefore, it was considered that the fine precipitates appearing on 673 K aging in the ferrite grain were of the same phase, regardless of the aging period. The fine precipitates during aging were dense in the simulated HAZ, but very thin in the parent castings. Annealing above 773 K gave sphere and rod precipitations, which gave electron diffraction spots consistent with a FCC of 1.21 nm lattice constant. EDS showed condensation of Ni, Si and Mo at the precipitates. But the electron diffraction spots were not enough for judgment of a crystal structure. Various types of precipitates are known to appear on annealing above 773 K (Ref. 5). Therefore, identification of the precipitates was difficult. The observed results are summarized in Table 2.

All CTOD data are shown only in the

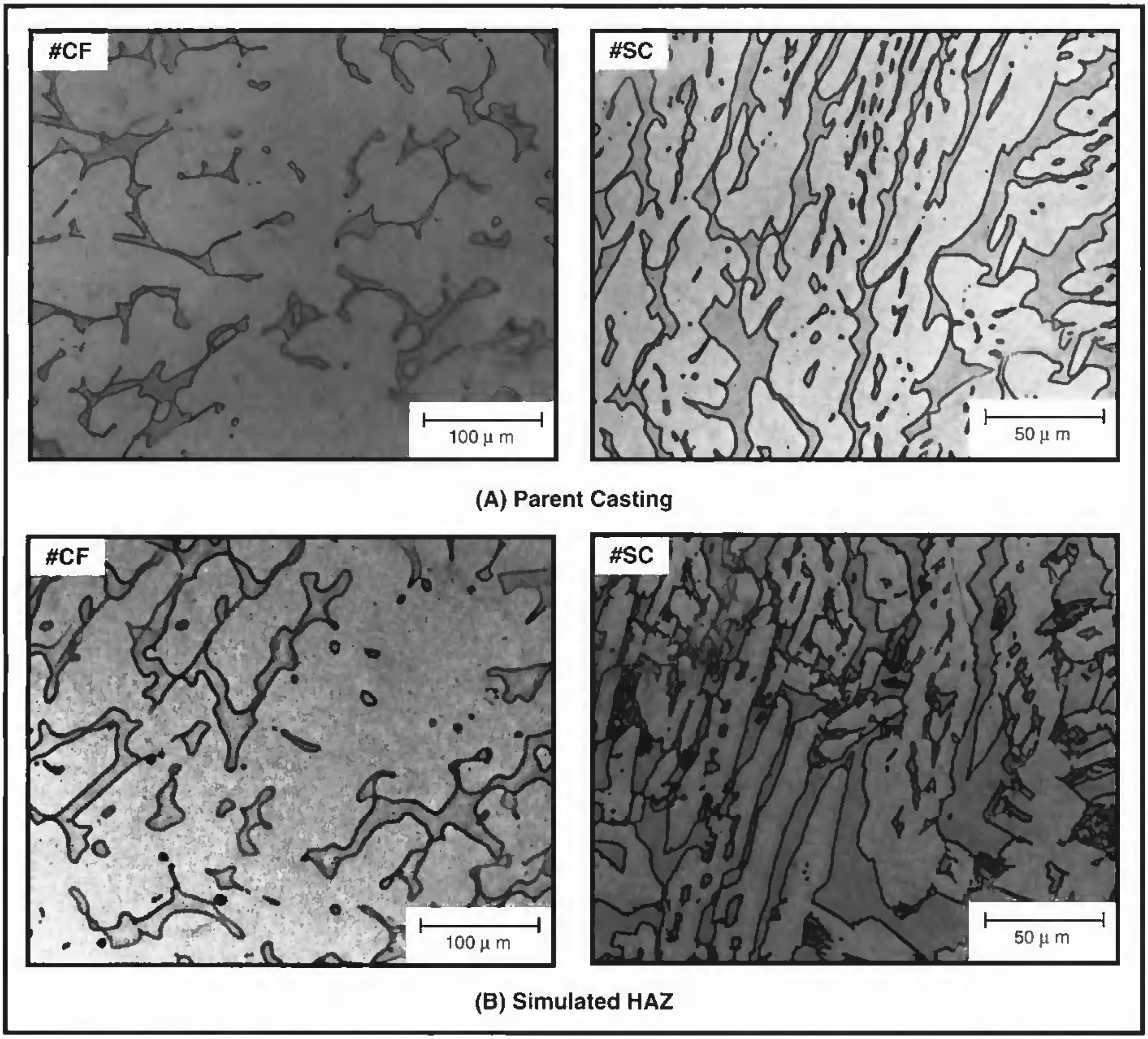

Fig. 3 — Microstructure of: A — Parent casting; and B — simulated HAZ subjected to a single cycle of cooling rate of 30 K/s in aged condition at 673 K for 28.8 Ms.

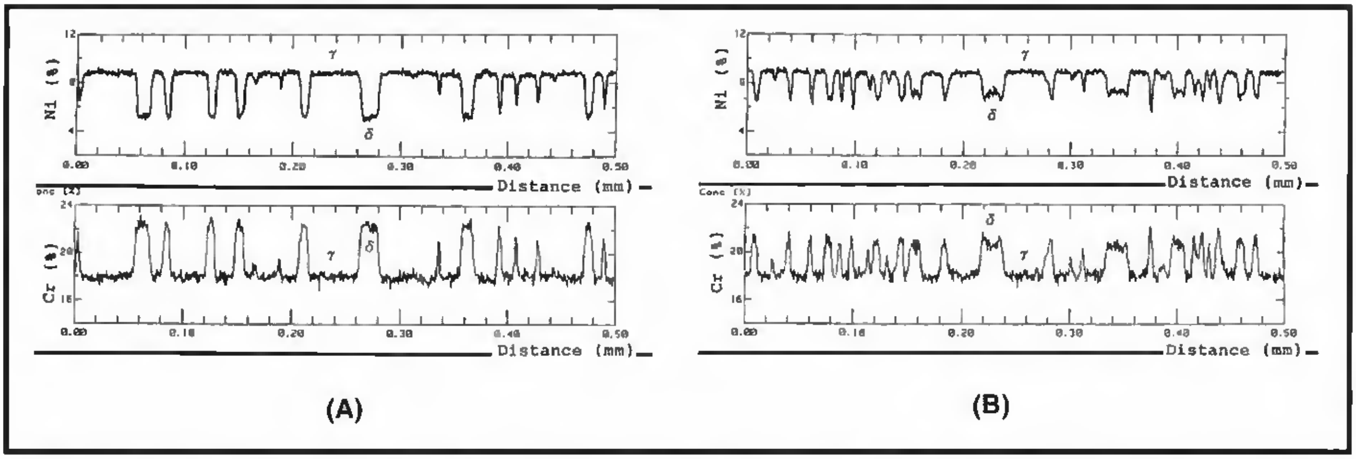

Fig. 4 — Distribution of alloy elements by EPMA line analysis for: A— Parent casting; and B — simulated HAZ subjected to a single cycle of cooling rate of 30 K/s in #SC.

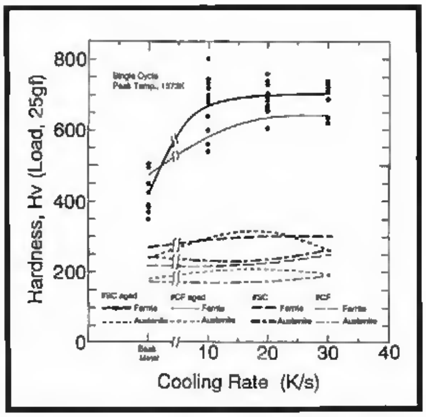

Fig. 5 — Microhardness of ferrite and austenite in parent casting and simulated HAZ of a single cycle for various cooling rates for #CF and #SC. Aging temperature: 673 K.

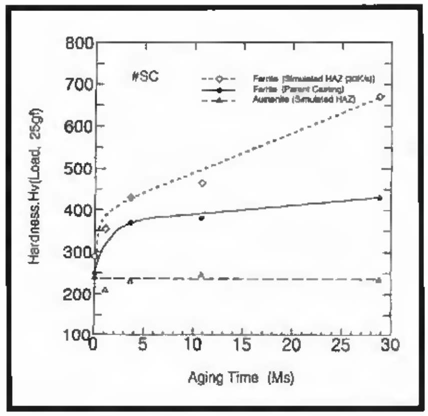

Fig. 6 — Microhardness of ferrite and austenite in parent casting and simulated HAZ of a single cycle for #SC as a function of aging period at 673 K.

form of transition curves in Figs. 8–12, except the few cases in which the measured values are plotted to show the CTOD scatter band. Distinction between δc and δu is made by suffixing c and u to the data points in the figure. No suffix data points represent δm. Arrows in the figures indicate that displacement was over the capacity for measuring the crack-mouth opening.

Figure 8 shows CTOD in #CF. The parent casting and the simulated HAZ had excellent toughness. Aging deteriorated toughness, especially for the simulated HAZ.

Figure 9A shows CTOD in #SC for various aging periods. As the aging period increased, CTOD of the parent casting and the simulated HAZ decreased. The decrease was more remarkable in the latter than in the former.

Figure 9B shows CTOD in #SC for various cooling rates of the simulated thermal cycle. The aged HAZ of #SC cooled in the rate of 30 K/s had the lowest CTOD. The embrittlement by aging was larger in #SC than in #CF.

Figure 10 shows CTOD in #SC subjected to the double cycle. The second cycle of the double cycle had little affect on the toughness of the simulated HAZ, except that the specimen subjected to the second cycle of the maximum temperature of 1173 K was somewhat inferior to the others in toughness. Deterioration by aging was rather lessened by application

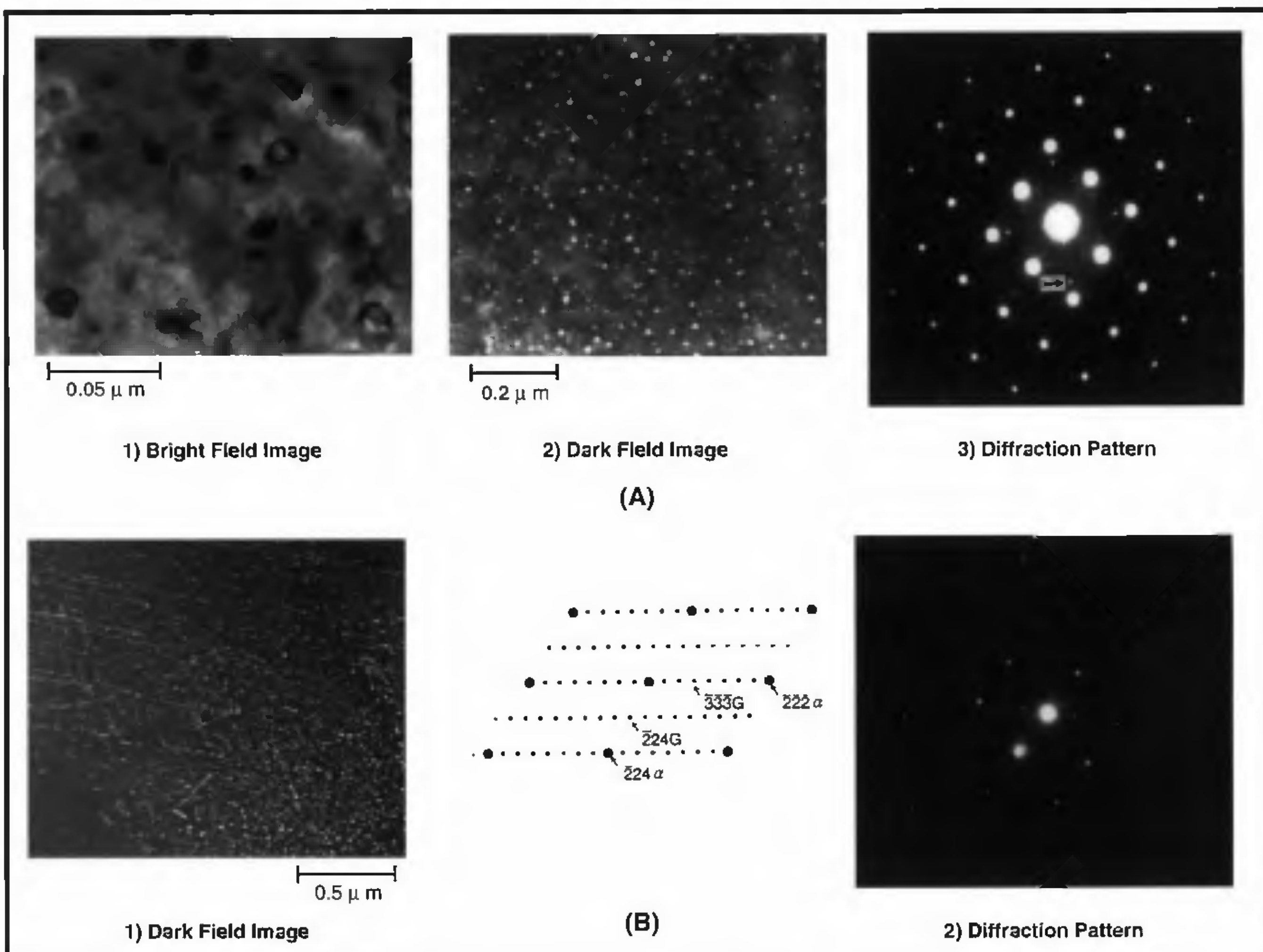

Fig. 7 — TEM observation of ferrite portion aged at 673 K for 28.8 Ms in: A — Simulated HAZ of a single cycle; and B — simulated HAZ of a double cycle. Main spots are due to ferrite. Subsidiary spots due to fine precipitates. Dark field images by one of the subsidiary spots are shown. Zone axes are 100 for Fig. 7A and 132 for Fig. 7B.

Table 2 — Summary of TEM Observations

Material	Thermal History	Aging Time (Ms)	Annealing	Precipitates in Ferrite Grain (density, size)	Precipitates at α/γ Boundary (size, St)
#CF	parent casting	28.8	no	very thin, ≤ 10 nm	~ 0.2 μm, $M_{23}C_6$
	single cycle (30 K/s)	28.8	no	dense, ≤ 10 nm	—
#SC	parent casting	10.8	no	nd	—
		28.8	no	very thin, ≤ 10 nm	~ 0.2 μm, $M_{23}C_6$
	single cycle (30 K/s)	no	no	nd	~ 0.03 μm
		1.08	no	nd	~ 0.2 μm, $M_{23}C_6$
		3.6	no	nd	—
		10.8	no	dense, ≤ 10 nm	~ 0.2 μm, $M_{23}C_6$
		28.8	no	dense, ≤ 10 nm	~ 0.3 μm, Laves phase $M_{23}C_6$
	single cycle (10 K/s)	28.8	no	thin – dense ≤ 10 nm	~ 0.2 μm, $M_{23}C_6$
	double cycle (1573 K, 1173 K)	28.8	no	thin ~ dense ≤ 10 nm	~ 0.2 μm, $M_{23}C_6$
	parent casting	28.8	773 K × 3.6 Ks	thin, ≤ 10 nm	~ 0.2 μm, $M_{23}C_6$
		28.8	773 K × 25.2 Ks	thin, 20 nm ~ 40 nm (sphere)	—
		28.8	873 K × 10.8 Ks	thin, 100 nm ~ 200 nm (rod)	—

no: not applied; nd: not detected; St: structure consistent with electron diffraction pattern

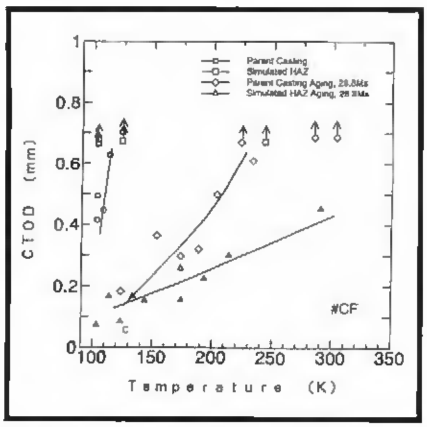

Fig. 8 — CTOD transition curves for parent casting and simulated HAZ of #CF that were as-heat treated or age hardened at 673 K. Marks with suffix c, u and without suffix represent δc, δu and δm, respectively, in all figures on CTOD from Fig. 8 to Fig. 12.

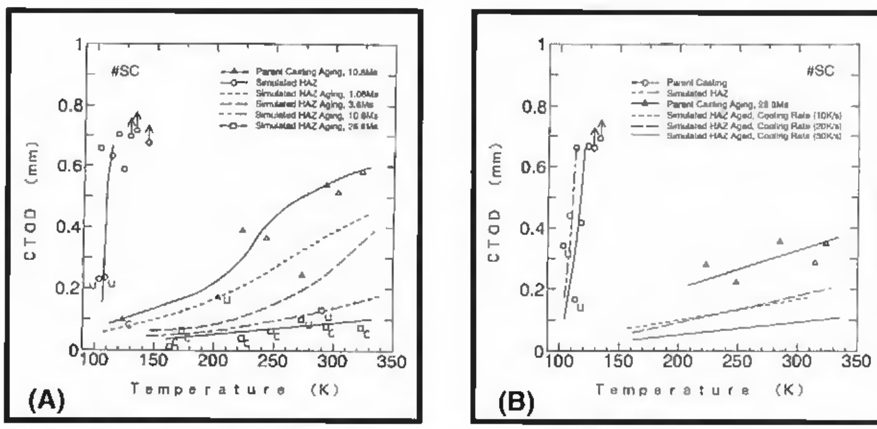

Fig. 9 — CTOD transition curves for parent casting and simulated HAZ of #SC that were as-heat treated or age hardened at 673 K: A — For specimens aged for various periods; and B — for specimens thermal cycled in various cooling rates and aged for 28.8 Ms.

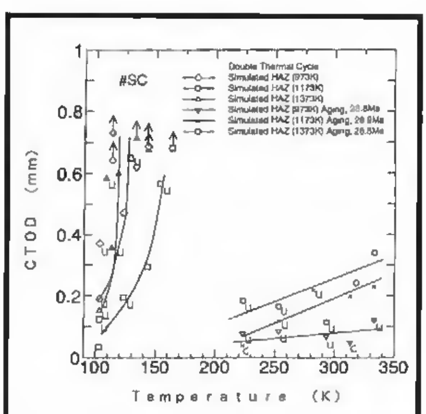

Fig. 10 — CTOD transition curves for simulated HAZ of double thermal cycles in #SC as-heat treated or age hardened at 673 K. Number in parentheses in the figure denotes the maximum temperature of the second cycle.

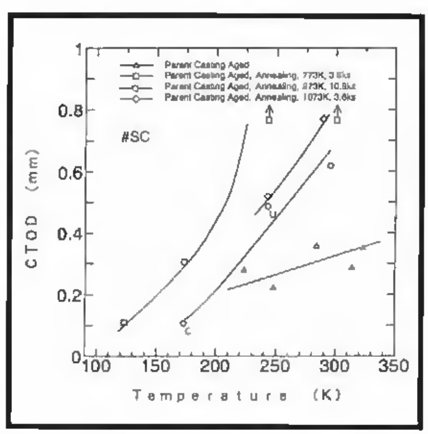

Fig. 11 — CTOD transition curves for #SC parent casting subjected to aging at 673 K followed by annealing under various conditions.

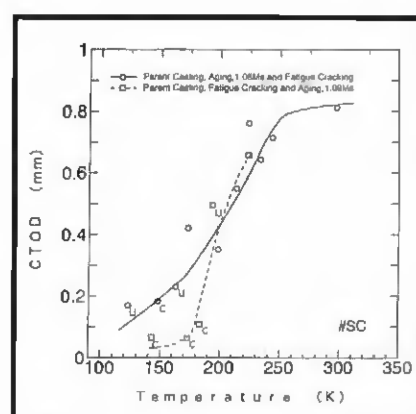

Fig. 12 — Comparison of CTOD transition curves between ordinary and reverse order of fatigue notching and aging at 673 K for 1.08 Ms in #SC parent casting.

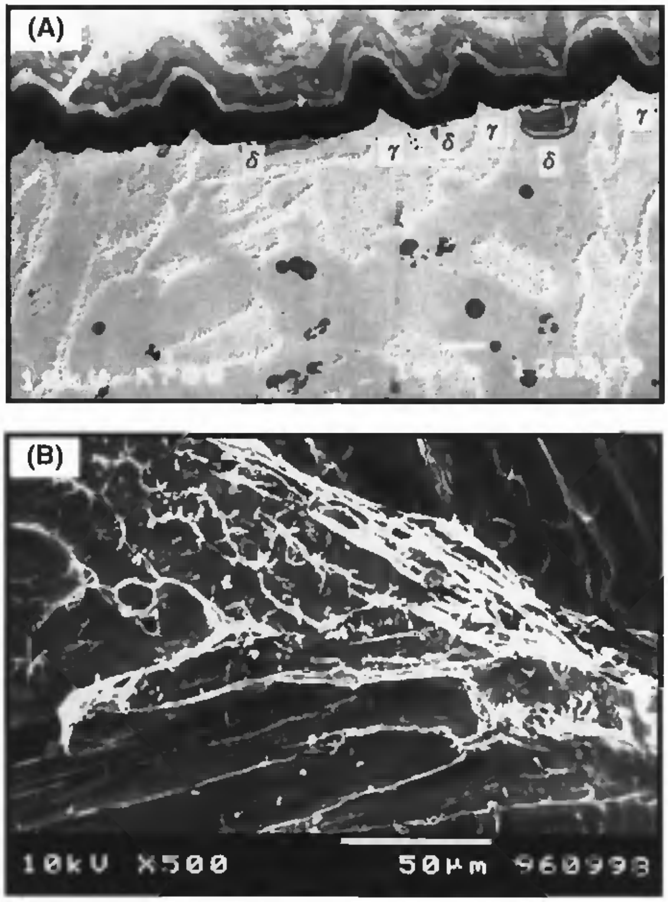

Fig. 13 — SEM observation for #SC simulated HAZ aged at 673 K for 28.8 Ms and tested at 323 K: A — Cross section of fracture surface; and B— fracture surface.

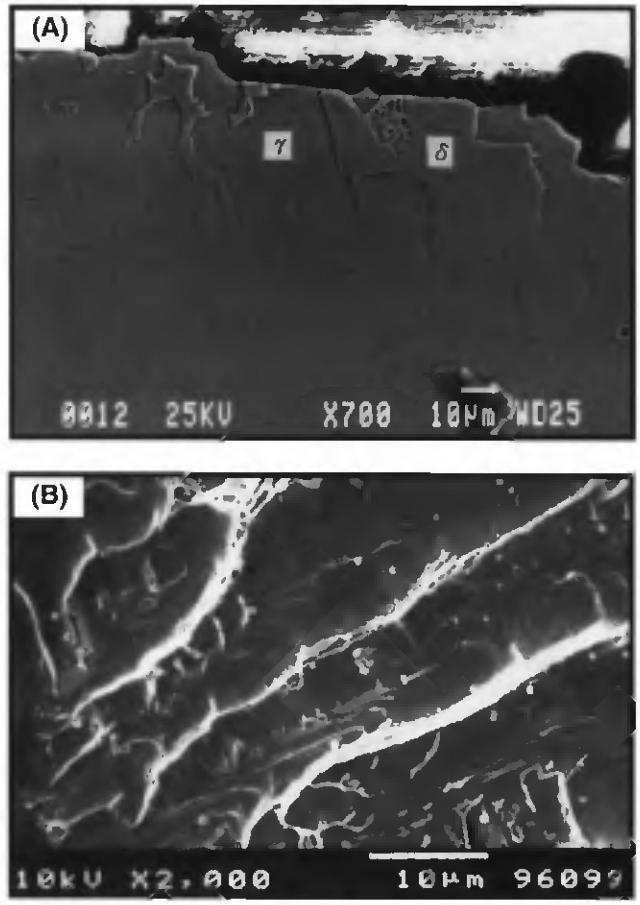

Fig. 14 — SEM observation for #SC simulated HAZ aged at 673 K for 28.8 Ms and tested at 163 K: A — Cross section of fracture surface; and B — fracture surface.

of the second cycle, except the specimen was subjected to the second cycle at the maximum temperature of 973 K.

Figure 11 shows the effect of annealing on the toughness in #SC parent casting embrittled by aging for 28.8 Ms at 672 K. The toughness recovered remarkably by annealing at 773 K for 3.6 ks. Prolonged annealing at the same temperature did not render further improvement in toughness.

Figure 12 shows the effect of changing the order of aging and fatigue notching on toughness using #SC parent casting. The test specimen prepared in the order of fatigue notching followed by aging gave more embrittlement than the usual procedure.

Microfractography with SEM and TEM was carried out mainly on the simulated HAZ of #SC aged for 28.8 Ms, *i.e.*, the highly deteriorated specimen, which showed an extremely brittle fracture appearance in a macroscopical view over the temperature range for CTOD testing.

SEM observation on section of a specimen tested at 323 K revealed that the austenite portion was broken, forming a tiny tearing ridge, while the ferrite portion fractured forming a flat facet on nearly the same plane as the neighboring fracture facets, as shown in Fig. 13A. On the contrary, in a specimen tested at 163 K, a considerable part of the austenite portion fractured in a flat plane, as shown in Fig. 14A. SEM photos of the fracture surface showed a more ductile appearance in Fig. 13B than in Fig. 14B, corresponding to the above cross-section observation.

TEM observation on the cross section of the fractured surface in a specimen tested at 223 K made it possible to identify the matrix phase neighboring the fracture surface by the electron diffraction method shown in Fig. 15. The upper part of the photo is plated Ni. In the right side of the photo, the crack propagated fairly flat, with creation of some stacking faults or epsilon martensite in the austenite portion. A dark field image using a austenite diffraction spot shows that austenite remained without martensitic transformation in a region apart less than 0.5 micron from fracture surface, though the martensitic transformation might have occurred in the region just adjacent to the fracture surface.

Highly preferred crystal orientation in ferrite was found both in the parent castings and the simulated HAZ, as shown by X-ray pole figure — Fig. 16. Preferred orientation was not recognized in austenite.

Discussion

It became clear from the present work that the HAZ of the cast austenitic stainless steels tends to deteriorate by aging more than the parent casting.

The aim of the present work is to explain why the thermal embrittlement is more pronounced for the simulated HAZ than for the parent casting.

It should be noted that the ferrite content and the hardness of the aged ferrite increased by application of the simulated welding thermal cycle. It has been noted in many previous papers that a specimen with higher content of ferrite suffers more deterioration by aging (Refs. 2, 6). Present results are consistent with this statement. Thermal embrittlement increased with the ferrite content, as seen in comparison

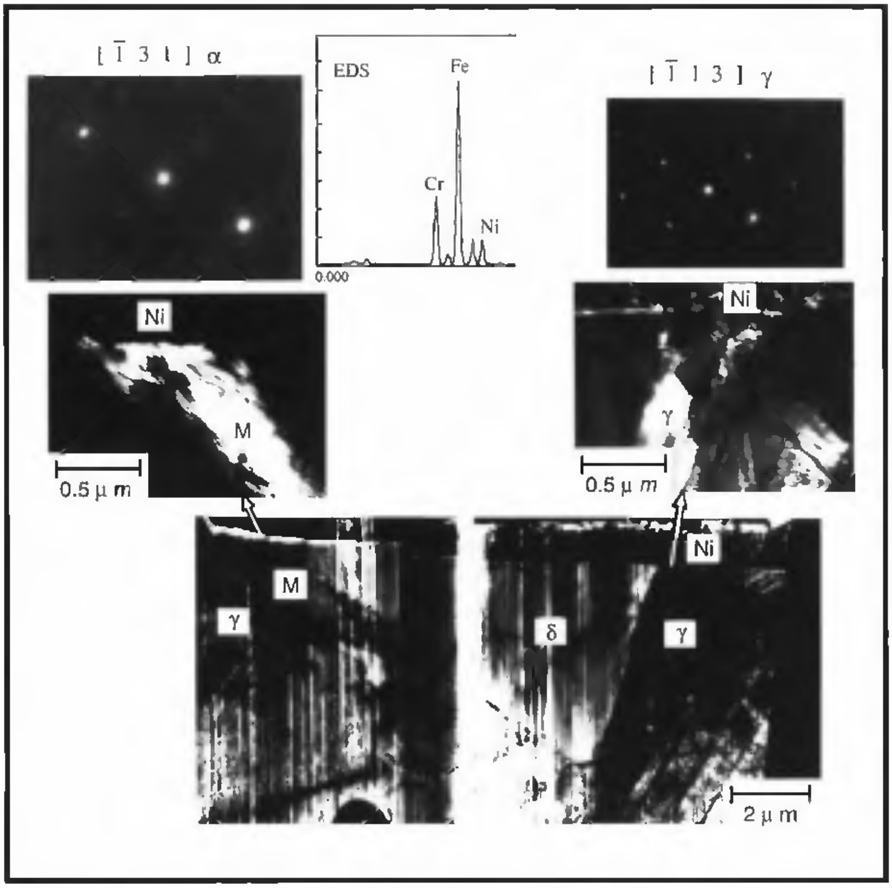

Fig. 15 — TEM observation of cross section of fracture surface for #SC simulated HAZ aged at 673 K for 28.8 Ms and tested at 223 K. Electron diffraction pattern from austenite portion is shown with its dark field image.

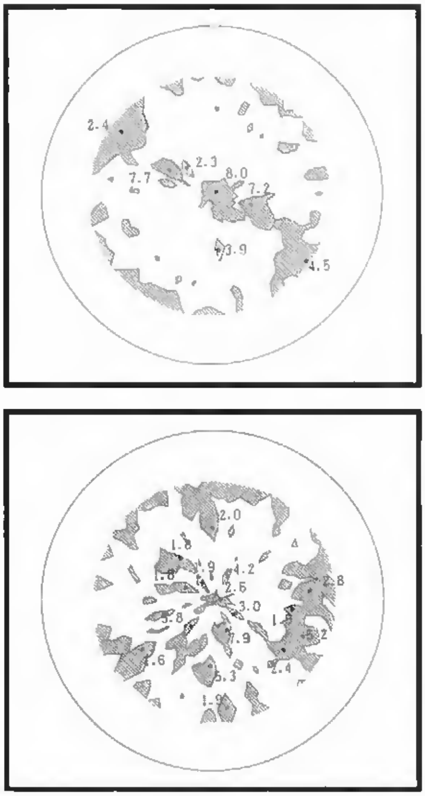

Fig. 16 — Example of 200 pole figure of: A — Parent casting; and B — simulated HAZ of a single cycle. Hatched area shows diffraction intensity higher than 0.5 times that of random orientation crystal. Numbers in the figure denote the maximum diffraction intensity at designated points.

between #CF and #SC, between the slow-cooled HAZ and the rapid-cooled HAZ, as well as between the parent casting and the simulated HAZ. The above rule is reasonable, because the higher content in ferrite, *i.e.*, the higher content of the matrix to be embrittled, the higher the susceptibility of the embrittlement.

Prior research also indicated that thermal embrittlement is induced by hardening of the ferrite matrix mainly due to spinodal decomposition. Precipitation of G phase might play some role on the hardening of ferrite (Ref. 2), though most researchers considered such roles negative (Ref. 3).

Fundamentals on spinodal decomposition and G-phase precipitation can be found in Ref. 7 and Refs. 8–10, respectively. There may be various changes by aging at 673 K in the metallurgical factors, such as reversion of ferrite to austenite and various types of precipitates mainly on grain boundaries, in addition to the spinodal decomposition and G-phase precipitation (Refs. 8–10). The reversion could not be recognized in the present study. The grain boundary precipitates were found for both the base metal and the simulated HAZ. The precipitates may cause microcrack, which is not necessarily the critical event for fracture with high resistance to propagation, as shown in Fig. 17.

Bonnet and others (Ref. 2) connected the above two empirical rules from the metallurgical viewpoint that an increase in ferrite-forming elements such as Cr, Si and Mo enhances both the spinodal decomposition and precipitation of G phase.

However, the parent casting and the simulated HAZ were prepared from the same cast. The cause for difference in ferrite hardness should be explained.

A direct proof for spinodal decomposition was not obtained in the present specimen. It is not necessarily easy to recognize spinodal decomposition by TEM, but it is reasonable to assume that the spinodal decomposition existed in the aged specimen. The increase in microhardness of ferrite in the early stage of aging for the parent casting and the simulated HAZ, as shown in Fig. 6, cannot be explained without the effect of the spinodal decomposition because precipitates were not found by TEM in the early stage of aging.

A cause of the increase in microhardness of ferrite in the latter stage may be explained by the following two mechanisms:

1) G-phase precipitation, and

2) further development of spinodal decomposition.

The increase in ferrite hardness showed good correspondence to the fine and dense precipitation presumably of G phase. This suggests that G-phase precipitation is the main cause of the difference in the age hardening and the thermal embrittlement between the parent casting and the simulated HAZ.

Contribution of G phase to the ferrite hardening in the parent castings has been denied in previous papers because:

1) Annealing at 823 K restored toughness by resolving only alpha prime phase, while G phase is stable up to about 900 K (Ref. 3)

2) a different amount of G phase between CF8 and CF8M did not give different behavior in aging (Ref. 10).

These explanations do not contradict the present assumption that the age hardening is remarkable only in the simulated HAZ.

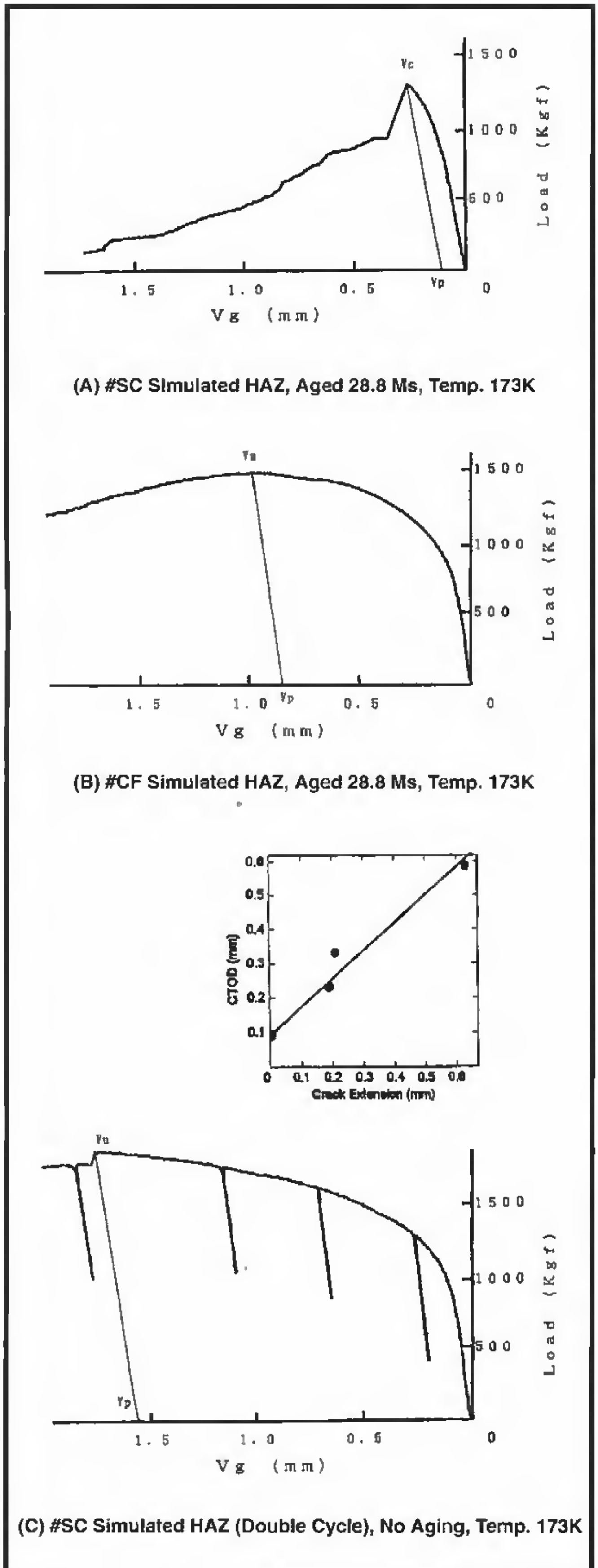

Fig. 17 — Example of load-crack mouth opening displacement curve in CTOD measurement with a CTOD-R curve in the last example.

As to the cause for the difference in the microstructure between parent casting and HAZ, the change of the metallurgical factors during thermal cycle and aging should be discussed. The parent castings received a thermal treatment at 1353 K or 1363 K for 10.8 Ks or 19.8 Ks, followed by water cooling. The simulated HAZ was subjected to an additional thermal cycle at 1573 K for 1 s. If the fraction of ferrite content, as well as its chemical composition, tends to change toward the equilibrium value of the phase diagram at the maximum temperature in both cases, it is assumed that the ferrite content will increase by application of the HAZ thermal cycle, though lowering of the cooling rate decreases the ferrite content a little due to possible transformation during a cooling period. It is also assumed that the ferrite matrix in the simulated HAZ has a lower Cr and a higher Ni content than in the parent castings, as seen from the phase diagram given in Ref. 11. This expectation corresponds well with present test results relative to the observation of the microstructure and EPMA measurement.

If the main controlling factor for spinodal decomposition is the chemical composition with regard to the miscibility gap spinodal decomposition, then the hardening by this cause might be expected to be less due to the lower Cr content in the simulated HAZ than in the parent casting (Ref. 2). This suggests that the higher ferrite hardness of HAZ cannot be explained without the contribution of G-phase precipitation to the hardness. More G-phase precipitation in the simulated HAZ may be expected by its higher Ni content than in the parent casting.

On the other hand, the high ferrite hardness in the simulated HAZ might be attributed to the alpha prime phase, which is the final stage of the spinodal decomposition, because addition of Ni was shown to accelerate the alpha prime appearance (Ref. 12). However, it is not certain whether the acceleration effect of Ni on the spinodal decomposition explains the higher age hardening in the simulated HAZ because of insufficient information in its mechanism and the condition for hardening. For instance, further promotion of the hardening by the increase in Ni content near 6% was not clear in the experiment by Nakano (Ref. 13). And G-phase precipitation was suggested to retard the spinodal decomposition by decreasing the Ni content in solution (Ref. 3).

More study is necessary for elucidation of the mechanism by which the simulated HAZ was more age hardened.

In addition to the metallurgical causes, geometrical effects on toughness should be examined. The problem is to explain why the aged, simulated HAZ fractured with a low CTOD in the macroscopically flat, *i.e.*, brittle fracture appearance, in spite of the existence of more than half of the ductile austenite portion. One possible explanation for this flat fracture surface may be the occurrence of brittle fracture for both the ferrite and austenite portions due to transformation from austenite to brittle alpha martensite at crack front on fracture, as suggested in Ref. 1. But this is not the case for the specimens tested at such a high temperature as 323 K, where austenite broke in a ductile manner, as shown in Fig. 13. In such a case, the flat fracture surface may be formed by the following mechanism.

The CTOD test pieces were machined from a columnar zone of the cast. The notch ligament of the test pieces had a crystal orientation in a columnar crystal and a texture over the columnar zone (Ref. 14). By heat treatment following casting, a considerable fraction of ferrite was transformed to austenite, and there was no heritage of the crystal orientation to the austenite. But the preferred crystal orientation was restored by the welding thermal cycle through growth of the ferrite of the same crystal orientation as that of the remaining ferrite. When the age-embrittled ferrite of high fraction with the highly developed preferred orientation was fractured, a skeleton of the macroscopically flat fracture surface formed first. In such a case, plastic deformation necessary for ductile crack formation in the austenite portion may be restricted within a region just near the crack plane due to constraint by the surrounding hard ferrite, resulting in formation of a tiny tearing ridge. Very little plastic deformation to cause ductile crack means a macroscopical brittle crack. In brief, the highly developed preferred orientation in the ferrite has two effects: promotion of cleavage in the ferrite portion and restraint of plastic deformation in the austenite portion by the formation of the flat plane.

In this respect, it is notable that the austenite matrix fractured in an apparent brittle manner at 223 K, as shown in Fig. 15. Though transformation to martensite may have occurred, it was highly localized near the crack path, which might be a result of the high restraint effect for plastic deformation by the hard ferrite around the austenite.

At such a low temperature as 163 K, sufficiently lower than Md point, the austenite portion can transform to martensite prior to crack propagation and fracture in a brittle manner as shown in Fig. 14.

Conclusion

Metallurgical controlling factors of embrittlement in HAZ of the cast austenitic stainless steels due to aging at 673 K up to 28.8 Ms were studied by using the simulated HAZ consisting of a single or double thermal cycle. The results are summarized as follows:

1) HAZ was more susceptible intrinsically to thermal embrittlement than the parent casting. The second cycle of the maximum temperature from 1173–1373 K reduced the susceptibility to some degree.

2) The higher susceptibility in the simulated HAZ was attributable to the higher age hardening and the more content in ferrite than in the parent casting.

3) The higher age hardening apparently had good correlation with a distribution of fine and dense precipitates in the simulated HAZ. The difference in precipitation behavior between the parent castings and the simulated HAZ may be attributed to a chemical composition change in ferrite induced by application of the welding thermal cycling.

4) A high fraction of the high hard ferrite was harmful to toughness by suppressing the austenite ductility, besides its brittle fracture behavior.

5) Annealing after aging, or exchange of the order of aging and fatigue cracking, had some effect on toughness.

Acknowledgments

The authors wish to thank Dr. H. Nakamura of JAPEIC for planning and leading this work in its early stage, Prof. Alexandre Kawano for his kind advice concerning the manuscript, H. Komatsu of Nittetsu Techno Research for TEM fractography and Top con Ltd. for the photo in Fig. 7A.

References

1. Strangwood, M., and Druce, S. G. 1990. Aging effect in weld cast CF3 stainless steel. *Material Science and Technology* 6: 237–247.

2. Bonnet, S., Bourgoin, J., Champredonde, J., Guttmann, D., and Guttmann, M. 1990. Relationship between evolution of mechanical properties of various cast duplex stainless steels and metallurgical and aging paramenters: outline of current EDF programmes. *Science and Technology* 6: 221–262.

3. Chung, H. M., and Leax, T. R. 1990. Embrittlement of laboratory and reactor aged CF-3, CF-8 and CF8M duplex stainless steels. *Material Science and Technology* 6: 249–264.

4. Spiegel, F. X., Bardos, D., and Beck, P. A. 1963. Ternary G and silicides and germanides of transition elements. *Trans. Met. Soc. AIME* 227: 575–579.

5. Auger, P., Danoix, F., Menand, A., Bonnet, S., Bourgoin, J., and Guttmann, M. 1990. Atom probe and transmission electron microscopy study of aging of cast duplex stainless steels. *Material Science and Technology* 6: 301–313.

6. Yukawa, S. Review and evaluation of the toughness of austenitic steels and nickel alloys after long-term elevated temperature exposures. *WRC Bulletin No. 378*, Welding Council.

7. Cahn, J. M. 1968. Spinodal decomposition. *Trans. AIME* 242: 166–180.

8. Vrinat, M., Cozar, R., and Meyzaud, Y. 1986. Precipitated phases in the ferrite of aged cast duplex stainless steels. *Scipta Metal.* 20: 1101–1106.

9. Vitek, M. K. 1983. G-phase formation in aged type 308 stainless steel. *Met. Trans. A.* 18A: 154–156.

10. Miller, M. K., and Bently, J. 1990. APFIM and AEM investigation of CF8 and CF8M primary coolant pipe steels. *Material Science and Technology* 6: 285–292.

11. Hayes, F. H., Hetherington, M. G., and Longbottom, R. D. 1990. Thermodynamics of duplex stainless steels. *Material Science and Technology* 6: 263–271.

12. Solomon, H. D., and Levinson, L. M. 1978. Moessbauer effect study of 475C embrittlement of diplex and ferritic stainless steels. *Acta Met.* 26: 429–442.

13. Nakano, K., Kanno, M., and Hoshino, A. 1978. Effect of nickel content and austenitic phase on low temperature toughness and embrittlement behaviour of Fe-26% Cr alloys. *Trans. Nat. Res. Inst. Metal* 20: 1–12.

14. *Metals Handbook*, 9th Edition. P. 700.

15. *ASTM E 1290-89*.

16. Joice, J. A. 1979. Computer Interactive J1c Testing of Navy Alloys. *ASTM STP* 668: 451–468.

17. McCabe, D. E. 1977. Determination of R Curve for Structural Materials using Nonlinear Mechanics Methods. *ASTM STP* 631: 245–266.

Appendix

CTOD

The critical CTOD, δc, is a kind of fracture toughness, such as the critical stress intensity factor K1c. The fracture toughness is the value of the parameter that characterizes the crack tip state at the onset of crack propagation. For δc, such a parameter is the crack tip opening displacement that is usually calculated from the crack mouth opening displacement, Vg, the critical value of which is expressed by Vc, Vu or Vm corresponding to the fracture behavior (Ref. 15).

Figure 17 shows examples of the record of the load vs. crack-mouth opening displacement in the present test. The value of δc is estimated from Vc shown in the upper part of the figure, δm from Vm in the middle part and δu from Vu in the lower part. In the last case, the compliance measurement by unloading on the load-displacement curve is shown together, which made it possible to estimate a crack extension using the equation by Sexena and Hudak (Ref. 16) and to depict CTOD-R curve as shown on the left lower side of Fig. 17. The gradient of the R curve is COA, which is a measure of the resistance to crack propagation.

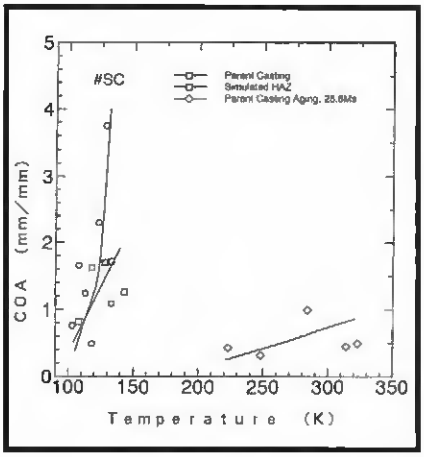

Fig. 18 — Example of COA transition curves.

In the transition temperature range, δm and COA increased with temperature. In contrast to the present results, COA in ordinary steels, *i.e.*, ferritic steels, does not depend on temperature even in the transition temperature range (Ref. 17). This difference can be explained in the following way: There is a correspondence between COA and δm, as seen from comparison between CTOD in Fig. 9 and COA in Fig. 18 for the aged parent casting. Despite macroscopically ductile fracture appearance of the aged parent casting, the stable crack extended with formation of cleavage microcracks as evidenced by the successive minute load drop on the load displacement curve. The resistance to apparent ductile crack extension, COA, decreases with increase in cleavage fracture fraction. Lowering of COA results in decrease in δm. Therefore, the decrease in δm with temperature was a result of the increase in cleavage fraction.